Si-Compatible Cleaning Process for Graphene Using Low-Density Inductively Coupled Plasma

Yeong-Dae Lim,[†] Dae-Yeong Lee,[†] Tian-Zi Shen,[†] Chang-Ho Ra,[†] Jae-Young Choi,[‡] and Won Jong Yoo[†,*]

[†]SKKU Advanced Institute of Nano-Technology (SAINT), Samsung-SKKU Graphene Center, Sungkyunkwan University, 300 Cheoncheon-dong, Jangan-gu, Suwon, Gyeonggi-do 440-746, Korea and [‡]Graphene Center, Samsung Advanced Institute of Technology, San 14, Nongseo-dong, Giheung-gu, Yongin, Gyeonggi-do 446-712, Korea

ABSTRACT

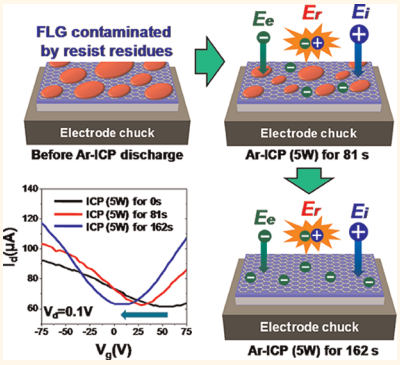

We report a novel cleaning technique for few-layer graphene (FLG) by using inductively coupled plasma (ICP) of Ar with an extremely low plasma density of 3.5×10^8 cm^{-3}. It is known that conventional capacitively coupled plasma (CCP) treatments destroy the planar symmetry of FLG, giving rise to the generation of defects. However, ICP treatment with extremely low plasma density is able to remove polymer resist residues from FLG within 3 min at a room temperature of 300 K while retaining the carbon sp^2-bonding of FLG. It is found that the carrier mobility and charge neutrality point of FLG are restored to their pristine defect-free state after the ICP treatment. Considering the application of graphene to silicon-based electronic devices, such a cleaning method can replace thermal vacuum annealing, electrical current annealing, and wet-chemical treatment due to its advantages of being a low-temperature, large-area, high-throughput, and Si-compatible process.

KEYWORDS: graphene · inductively coupled plasma · cleaning · field effect transistor · charge neutrality point · silicon processing

While graphene has been surprisingly compatible with most complementary metal oxide semiconductor (CMOS) processes, there remain key issues that must be resolved before integration into device fabrication, *e.g.*, damages induced by reactive ion etching and/or photoresist ashing, and compatibility of photoresists with graphene. Due to the atomic layer thickness of graphene, reactive ions, especially oxygen, cause damage to the crystal structure of graphene. Graphene, a one-atom-thick layer of graphite,[1−3] is extremely sensitive to device-processing environment, which can result in the change of its intrinsic properties, compared to silicon of bulk structure.[4,5] The typical lithography process for fabricating graphene devices leaves polymer resist residues on the graphene surface,[6] giving rise to unintended change of electrical properties such as shift of the Fermi level and decrease of carrier mobility.[7] To date, thermal annealing,[7−9] electrical current annealing,[10,11] and chloroform treatment[8] were introduced to remove polymer contaminants. However, metal as electrode is easily damaged by high-temperature (∼200 °C) thermal annealing of long duration (∼10 h). Such high temperature results in the generation of radicals by random scission of polymer, which brings about reactions between radicals and graphene defects.[12] Electrical current annealing also removes contamination of the local area of graphene, but it is found difficult to remove contamination of the large area of graphene. Chloroform, as a toxic anesthetic, is an inadequate solvent for industrial applications because it is harmful to the environment. Therefore, the development of a novel restoration technique for graphene that has undergone device processes is of utmost importance.

The previous plasma studies have documented techniques aimed at controlling the properties of graphene, such as decoration,[13] growth,[14,15] functionalization,[16,17] etching,[18,19] doping,[20,21] band gap,[22] and surface conditions.[23−26] However, such works revealed that the generation of defects is inevitable during the plasma process. These works[15−26] involved at least one of the following for the treatment of graphene: (1) a capacitively coupled plasma (CCP) source, in a

* Address correspondence to yoowj@skku.edu.

Received for review March 13, 2012 and accepted April 19, 2012.

Published online April 20, 2012
10.1021/nn301093h

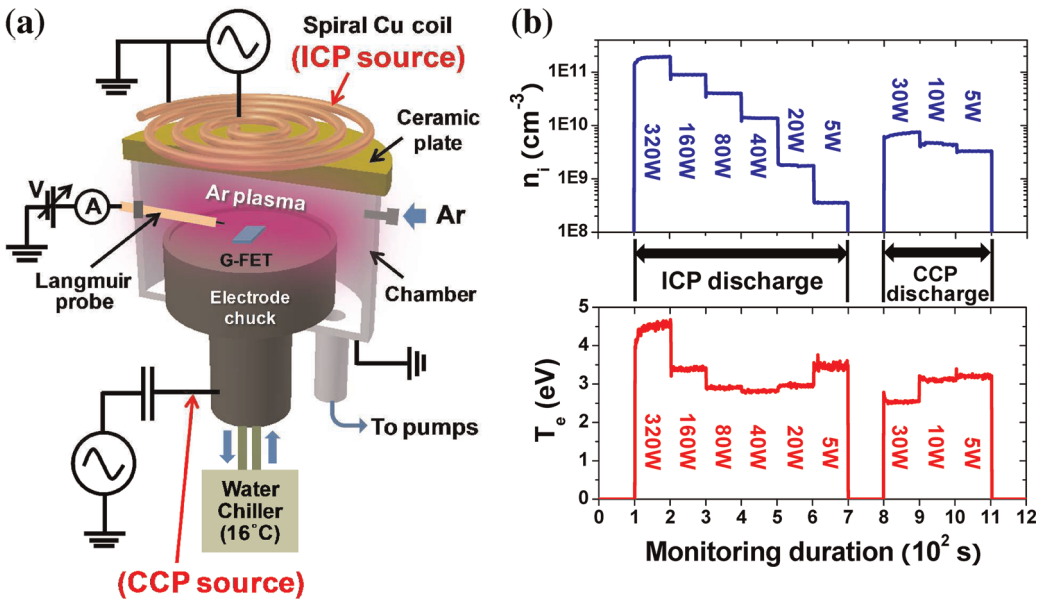

Figure 1. (a) Schematic of plasma reactor. Diameter of electrode chuck is 200 mm, and distance between electrode chuck and ceramic plate is 90 mm. (b) *In situ* monitoring of ion density (n_i) and electron temperature (T_e) for various Ar plasmas by using a Langmuir probe system.

process usually referred to as reactive ion etching (RIE); (2) a high-density plasma discharged by high rf power; and (3) gaseous O_2 or H_2. However, we believe that these plasma conditions are directly responsible for inducing damage in graphene. This is because CCP induces very high ion bombardment energy, high-density plasma causes a high ion density, and O_2 or H_2 easily reacts with carbon. For these reasons, a new plasma, which is entirely different from the previous ones, should be introduced in order to achieve successful plasma processing without generating defects in graphene.

Here, we report the first experimental study of a few-layer graphene (FLG) cleaning method that can be integrated into a graphene field effect transistor (G-FET) to remove polymer resist residues by using argon inductively coupled plasma (Ar-ICP)[27] in the extremely low density range. According to the electrical characterization results, the mobility and charge neutrality point (V_{np}, also referred to as the Dirac point) of G-FET are restored to those of pristine FLG without defects, after the G-FET is exposed to the ICP. Such a cleaning method compatible with Si processing[28] is more advantageous than thermal annealing in that it can be operated as a low-temperature (near room temperature; see the Methods for details about temperature increase of graphene by the ICP) and high-throughput process (~100 times faster than vacuum thermal annealing). It also has an advantage over electrical current annealing in that it can be applied to a large surface area.

RESULTS AND DISCUSSION

Figure 1a shows a schematic diagram of our G-FET staged at the electrode chuck in the plasma reactor. Figure 1b shows the diagnosis results of Ar plasma by using a Langmuir probe system. (See Methods for details about device fabrication, plasma reactor, experimental process, and plasma diagnosis.)

Figure 2a shows atomic force microscopy (AFM) topographic images of FLG exposed to ICP as a function of exposure duration. Here, the rf power of ICP is fixed at 5 W. When pristine FLG, freshly cleaved on the SiO_2 (see image A), is used to fabricate the G-FET, resist residues are left on FLG (see image B), leading to the increases of the RMS roughness and thickness by as much as 1.07 and 5.1 nm, respectively (see Figure 2b,c). When the G-FET is exposed to ICP (5 W) for 81 s, the RMS roughness is 1.04 nm and the thickness of FLG (see image C) is 4.2 nm. When the G-FET is exposed to ICP (5 W) for 162 s, both the RMS roughness and thickness of FLG (see image D) are restored similar to those of the pristine FLG (see image A) because the resist residues are removed by the ICP treatment. When the G-FET is exposed to ICP for an extended duration of 486 s, the RMS roughness and thickness of FLG (see image E) show no further decrease.

Figure 3a shows the Raman spectra of a graphene before and after plasma treatment. The absence of a D-band at ~1350 cm^{-1} indicates that there is no damage to the planar sp^2 structure of FLG induced by low-density ICP (5 W) treatment even up to 486 s. When the G-FET is exposed to ICP (40 W) for 162 s, a D-band appears, and the intensity of the 2D-band decreases. Figure 3b shows intensity ratios between D-band and G-band as a function of time for various ICP powers. According to the result, it is understood that the generation of defects in FLG is observed dependent on ICP exposure duration except for low-density

ICP (5 W), where no D-band is observed for the entire duration, up to 486 s. In contrast, when G-FET is exposed to CCP (5 W) for 27 s, the planar sp^2 carbon structure is almost destroyed, resulting in the removal of FLG.

The following explains the behavior of the particles in the plasma, based on the experimental results. Figure S1a (see Supporting Information) shows their behavior in the CCP discharged by a power of 5 W. When V_b is applied to the electrode chuck, a plasma sheath is formed nearby. The thickness of the sheath in our CCP appears to be ~1.5 cm by optical inspection, although it is estimated to be only ~0.26 cm if the formula from dc plasma is used.[29] Most of the electrons are present outside of the sheath.[30] It is understood that the energy supplied to graphene is mainly attributed to ion bombardment (Ar^+) in CCP treatment.[22] Kinetic energy (E_i) of bombarding ions is assumed by the potential difference as $V_p - V_b$, where V_p and V_b are plasma potential and negative bias voltage, respectively. In the CCP process, a V_b of hundreds of volts is applied to the electrode chuck, resulting in an E_i of hundreds of eV. On the other hand, according to atomistic computer simulations a minimum kinetic energy of Ar atom of ~32 eV is required for displacing one carbon atom from pristine graphene.[31] Therefore, we think that a sufficiently high energy E_i transferred to the FLG in CCP is available to destroy the sp^2 bonding of FLG (see Figure S1c), although the accelerated ions are subject to collisions with neutral particles in the sheath, which results in a decrease of bombardment energy (see Figure S1a).[32]

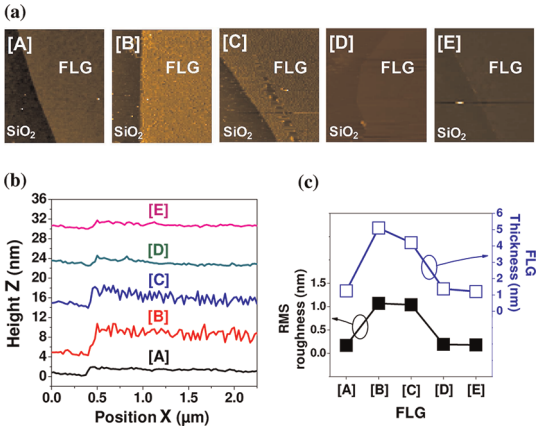

Figure 2. AFM analysis of FLG. (a) Surface morphologies of FLG used for G-FET after treatment of ICP (5 W). Here [A] is pristine FLG, [B] is FLG applied to FET (before plasma treatment), and [C], [D], and [E] are graphene exposed to ICP (5 W) for 81, 162, and 486 s. (b) Surface profile scans from [A] to [E]. (c) RMS roughness and thickness from [A] to [E].

Figure 4a shows the behavior of the particles in the ICP. The FLG placed on the electrode chuck is in the ground state (V_0 = 0 V), and no CCP power (P_{CCP}) is applied. (Note that in this state both ions and electrons can be introduced to the FLG.) The sheath thickness from our low-density ICP condition is estimated to be ~0.17 cm if the formula from dc plasma is used,[29] which is thinner than the sheath thickness of ~1.5 cm formed by CCP using Ar. The energy E_i is only determined by V_p, as V_0 is 0 V. In ICP, V_p is normally diagnosed to be 10−20 V,[33,34] resulting in 10−20 eV for the E_i. Therefore, a maximum E_i of 10−20 eV can be supplied to FLG if energy loss originating from collisions in the sheath is ignored. Such energy is smaller than ~32 eV, which is the minimum kinetic energy of bombarding ions for displacing one carbon atom as mentioned above, resulting in no defect generation of FLG exposed to ICP (5 W).

Note that the E_i changes little as a function of ICP power (P_{ICP}) due to the V_p changing little in various P_{ICP}.[33]

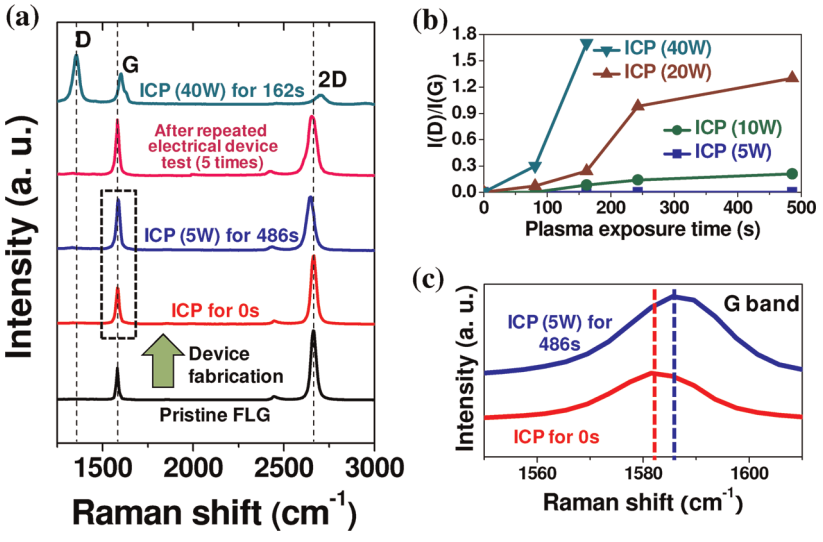

Figure 3. (a) Raman spectra of FLG obtained after various plasma treatments. Black dotted rectangle is enlarged in (c). (b) Intensity ratio of D-band and G-band, *I*(D)/*I*(G), of FLG for various plasma conditions. (c) Zoom-ins of Raman G-band of FLG exposed to ICP (5 W) for 0 and 486 s.

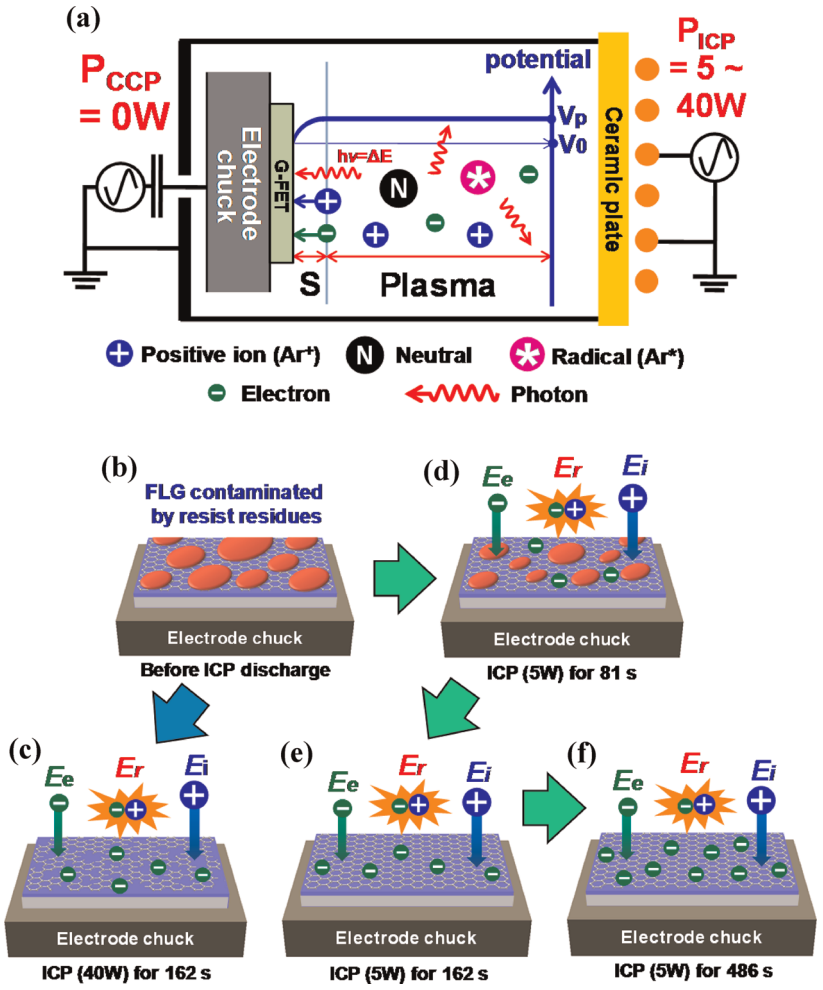

Figure 4. Schematic description of behaviors of plasma particles during ICP treatment for FLG. (a) Behavior of particles present in ICP. S denotes sheath. (b) FLG modified by reactions with resist residues before plasma treatment. (c) ICP (40 W) treatment for 162 s. ICP (5 W) treatment for 81 s (d), 162 s (e), and 486 s (f). Electron flux (J_e) is transferred to the FLG surface, resulting in a charging effect.

However the D-band is detected from the FLG treated with more than 10 W of P_{ICP} (see Figure 3a,b). We think that energy other than the E_i is responsible for the generation of defects with increasing P_{ICP} and plasma exposure time t. It was documented that main energies transferred to the substrate exposed to ICP with zero negative bias voltage (P_{CCP} = 0 W) are the following: (1) kinetic energy of bombarding positive ion and (2) energy released by electron−ion recombination near the substrate surface.[34] Here, E_r as the thermal energy generated by the recombination between Ar^+ and electron is considered to be the same as the ionization energy of Ar, which is 15.8 eV.[34] Therefore we think that the total energy deposited to FLG by ICP, U, can be accumulated in the FLG and released after it reaches the energy capacity of FLG.

Detailed descriptions of cleaning of residues by ICP (5 W) are as follows: Normally photoresist residues consist of the polymers novolac as base resin and diazonaphthaquinones as sensitizers.[36] However, for graphene nanoscale device fabrication employing electron beam lithography, poly(methyl methacrylate) (PMMA) is used as the pattern mask. PMMA is also used as the "handle" layer to form CVD graphene.[37] All of such polymers contain O atoms.[36,38] When the G-FET is exposed to Ar-ICP, resist residues on FLG are subject to E_i (ion bombardment energy) and E_r (recombination energy). We think that thermal energy induced from E_r brings about oxidation of resist residues via O atoms contained in such polymers. When the ICP (5 W) is exposed to G-FET, residues are subject to the E_i and E_r, resulting in removal of residues (see Figure 4d,e). At the same time, electrons incident on the graphene from ICP are trapped (see Figure 4d−f). In ICP, energies of incident electrons (E_e) and photons ($h\nu$) are considered to be negligible due to much smaller energy compared to E_i and E_r.[34,35]

Figure 5 shows an analytical model of various energy components transferred from ICP to the FLG with resist residues. The energy (E) provided by each ion from the events of ion bombardment (E_i) and recombination

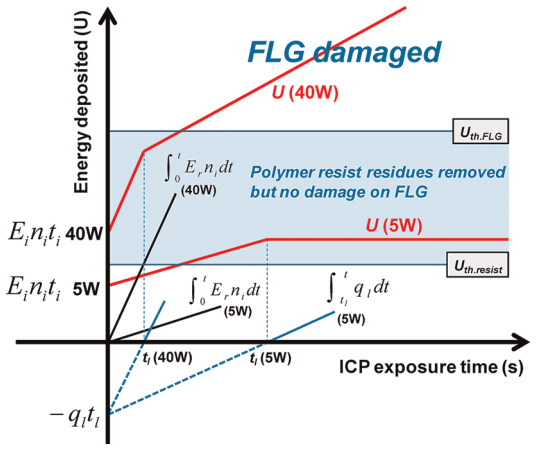

Figure 5. Schematic model of energy transferred to the FLG contaminated with resist residues.

with electrons (E_r) is

$$E = E_i + E_r \quad (1)$$

The total energy deposited (U) over time (t) for unit area is

$$U = E_i n_i(P_{ICP}) t_i + \int_0^t E_r n_i(P_{ICP})\, dt - \int_{t_l(P_{ICP})}^t q_l\, dt \quad (2)$$

where t_i is the time taking for a solid atom to lose energy to neighbor atoms after a bombarding ion collides with the solid atom, n_i is the ion density as a function of ICP power, t_l is the time for the solid atom to begin releasing energy after saturation of heat capacity as a function of n_i (P_{ICP}), and q_l is the energy releasing rate of a solid per unit volume. In eq 2, we think that ion bombardment energy ($E_i n_i t_i$) is only deposited to an atom for t_i because it is transferred to neighbor atoms, similar to the model of billiards, whereas recombination energy ($\int_0^t E_r n_i\ dt$) continues to be deposited, although deposited energy exceeding the capacity of the solid is lost ($\int_{t_l}^t q_l\ dt$). Since ICP exposure duration (t) is usually much longer than t_i, *i.e.*, $t \gg t_i$, eq 2 becomes

$$U = [E_r n_i(P_{ICP}) - q_l]t + q_l t_l(P_{ICP}) \quad (3)$$

.

Here, we interpret eq 3 as that U remains unchanged when energy flux supplied by recombination to the solid is smaller than its energy releasing rate (*e.g.*, ICP power of 5 W), *i.e.*, $E_r n_i(P_{ICP}) \le q_l$, whereas it keeps increasing if $E_r n_i(P_{ICP}) > q_l$. The above results can be described by the schematic model shown below: U is a function of ICP power (n_i) and time (t), where $U_{th.resist}$ is the threshold energy required to remove resist residues and $U_{th.FLG}$ is the threshold energy required to damage FLG. Note that t_i is very small compared to the time scale used in our experiment, and thus it is not shown in the diagram.

According to the model proposed above, we think that an ICP power of 5 W induces energy to be deposited onto the FLG, which stays between $U_{th.resist}$ and $U_{th.FLG}$, and thus resist residues are removed while FLG is not damaged. However, an ICP power of 40 W induces energy deposition onto the FLG, which increases with time so as to exceed $U_{th.FLG}$, and thus FLG is damaged (see Figure 4c).

Figure 3a shows that the G and 2D bands of FLG are up-shifted by 4 cm^{-1} (see Figure 3c) and down-shifted by 12 cm^{-1}, respectively, after ICP (5 W) treatment of the G-FET for 486 s. According to the previous report, the origins of the band shifts of G and 2D could be variations in the strain,[39] temperature,[40] and doping of graphene.[5,8,9] The exfoliated FLG used in this study, which was deposited on SiO_2 and exposed to plasma, does not easily undergo tensile or compressive strains. When the temperature of graphene increases, the G-band is down-shifted,[40] which disagrees with our results in terms of the shift direction. Here we attribute the upshift of the G-band and the down-shift of the 2D-band to negative charge transfer caused by the current J_e, which is trapped on the surface of FLG by the ICP. A more detailed description is as follows. As mentioned above, both J_e (electron flux) and J_i (ion flux) from the plasma into the grounded electrode where FLG is placed are the same. Electrons are more thermally active compared to other neutral particles present in the plasma, and these active electrons can be attached on the FLG surface, called plasma induced charge damage (PID). It is understood that PID is prevalent from ICP where electron temperature (T_e) is in the range of 2.8−4.7 eV (see Figure 1b). Our assessment is supported by a previous study,[9] which reported that the G-band is up-shifted due to electron and hole doping, while the 2D-band is down-shifted (up-shifted) due to electron (hole) doping. When the G-FET was exposed to ICP (40 W) for 162 s, the carbon sp^2 bonding of FLG broke and sp^3-hybridized bonding was generated, which easily absorbed the oxygen, hydrogen, and moisture, causing p-doping and upshift of the G- and 2D-bands by as much as 16 and 48 cm^{-1}, respectively.[5,24]

The following explains the electrical properties of the G-FET treated by various plasma conditions. A schematic illustration of our back-gated G-FET and optical image of this device are shown in Figure 6a. The effects of plasma treatment on the electrical properties (I_d−V_d) of the G-FET are shown in Figure 6b. The current level slightly fluctuates by low-density ICP of 5 W up to 486 s due to left-shift of V_{np}, as shown in Figure 6c,d. In contrast, when the G-FET is exposed to ICP of 40 W for 162 s, the current level dramatically decreases due to defect generation in FLG, as shown in Figure 3a. CCP entirely removes FLG, resulting in no current conduction in G-FET.

Figure 6c shows the electrical properties (I_d−V_g) of the G-FET after ICP (5 W) treatment for 0, 81, and 162 s. In our case, V_{np} is 54 V before plasma treatment

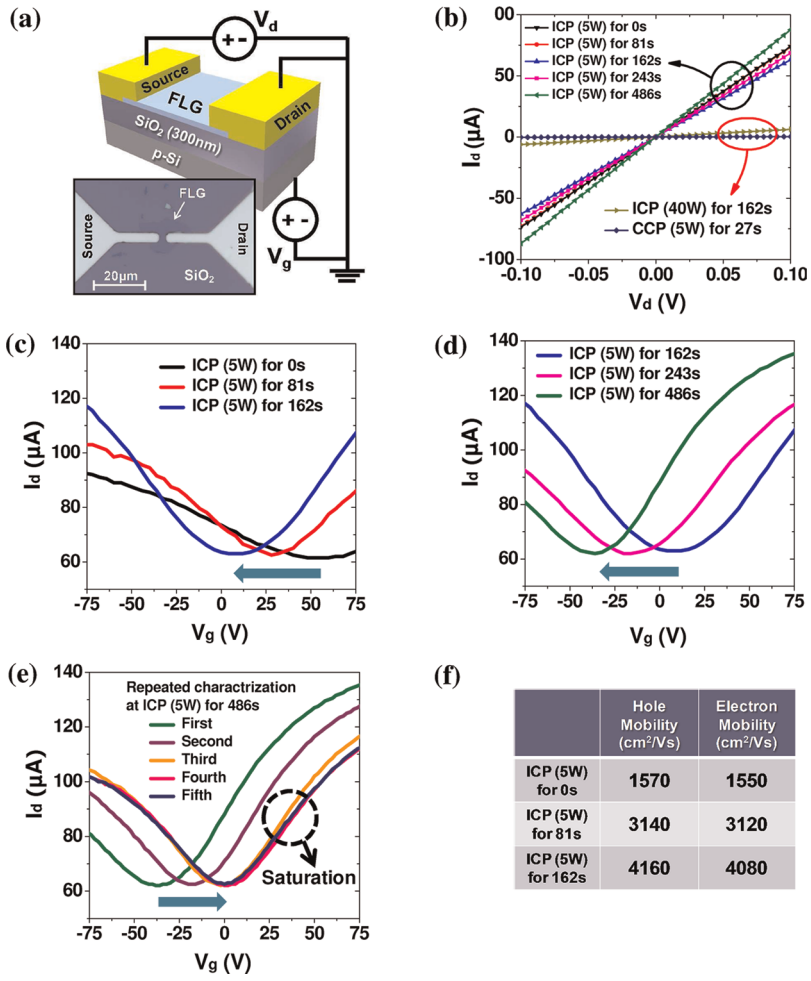

	Hole Mobility (cm^2/Vs)	Electron Mobility (cm^2/Vs)
ICP (5W) for 0s	1570	1550
ICP (5W) for 81s	3140	3120
ICP (5W) for 162s	4160	4080

Figure 6. (a) Schematic of back-gated G-FET and optical image. (b) I_d-V_d (V_g = 0 V) of G-FET obtained from various plasma sources (ICP or CCP), powers, and exposure times. I_d-V_g (V_d = 0.1 V) after ICP (5 W) treatment for (c) 0, 81, and 162 s and (d) 162, 243, and 486 s. (e) I_d-V_g after repeated characterization at 486 s. (f) Carrier mobilities obtained after ICP (5 W) treatment for 0, 81, and 162 s.

because the resist residues remaining on the FLG (see Figure 2a, image B) cause heavy p-doping of the graphene. V_{np} is found to be 27 and 8 V after 81 and 162 s of plasma exposure, respectively. The carrier mobility (μ) shown in Figure 6f can be deduced by $\mu = [(\Delta I_d/V_d)(L/W)]/C_{ox}\Delta V_g$, where L and W are the length and width of the channel, respectively, and C_{ox} is the silicon oxide gate capacitance ($C_{ox} = 1.15 \times 10^{-8}$ F/cm^2 for 300 nm thick SiO_2[24]). Removal of the resist residues (see Figure 2a, images C–E) by ICP (5 W) treatment causes a decrease of the carrier scattering in FLG, resulting in an increase in both the electron and hole mobilities.

Figure 6d shows the I_d-V_g values obtained after ICP (5 W) treatment of the G-FET for 162, 243, and 486 s. As mentioned earlier, V_{np} is 8 V for 162 s of treatment, −18 V for 243 s, and −37 V for 486 s. The J_e induced on the surface of the FLG (see Figure 4d–f) is responsible for the shift of V_{np}, which leads to the negative charging of FLG.

Figure 6e shows the results (I_d-V_g) of characterization experiments that were repeated five times by using a G-FET showing a V_{np} of −37 V after ICP (5 W) treatment for 486 s. Each characterization takes ~30 s. V_{np} shifts to near 0 V after the repeated tests and then does not shift anymore. For example, when the graphene is put into contact with metal, electrons in the metal are transferred to graphene due to the difference between the work functions, resulting in a Fermi level shift and n-doping.[41,42] However, in our case, FLG is only temporarily charged by J_e while the plasma is turned on. Therefore, V_{np} is restored to near 0 V as the pristine and neutral state of FLG. When a permanent n-doping process is induced by the NH_3 plasma, the intensity of the D-band increases due to breaking of the sp^2 bonding, which becomes equivalent to doping with impurities.[20] In contrast, the D-band is not observed after ICP (5 W) treatment for 486 s, while the position of the 2D-band is restored to that of the pristine FLG after the five repeated electrical tests: see Figure 3a. This indicates that the ICP treatment causes a temporary charging effect without impurity doping. On the other hand, it is well known that

particulates (O in particular) can be easily adsorbed on the graphene surface, causing a p-type effect.[5] However, we tried to minimize the particle-absorbing effect by conducting the electrical measurements immediately after the plasma treatment (see Methods: Experimental Process). If the particle-absorbing effect were a dominant reason responsible for Figure 6e, V_{np} should have exceeded 0 V toward the positive side by repeated electrical tests. However, our result in Figure 6e shows the saturation of V_{np} near 0 V instead, retaining the neutral state of FLG. Therefore, we conclude that the particle-absorbing effect is overcome and the FLG charged temporarily by electrons is restored to the neutral state via repeated electrical tests.

CONCLUSION

In this study, an ICP treatment with a very low plasma density ($<5 \times 10^8$ cm^{-3}) using Ar is proposed to restore FLG to its pristine state without generating defects. It is confirmed that the unwanted doping of holes in FLG that is caused by the fabrication process is removed by the ICP treatment. It is found that the ICP cleaning process presented in our work is feasible for low-temperature, large-area, high-throughput, and Si-compatible graphene device processes.

METHODS

Sample Preparation and Measurements. FLG flakes were deposited through micromechanical exfoliation of highly ordered pyrolytic graphite on p-doped Si substrates covered with a 300 nm thermally grown SiO_2 film. The thickness and RMS roughness of freshly cleaved FLG are 1.2 and 0.17 nm, respectively (see Figure 2a–c, image A). Standard photolithography is performed to fabricate the devices, using Pd (45 nm) lift-off metalization. Photoresist was removed by acetone in the lift-off process. The electrical properties of these devices were measured using a semiconductor analyzer at room temperature and atmospheric environment. Atomic force microscopy was used to investigate the image, profile, and roughness of the FLG surface. Raman spectroscopy of 514 nm excitation was performed to determine the transitions of bonds, defects, and doping of FLG.

Descriptions of Plasma Reactor and Its Diagnosis. Figure 1a illustrates the plasma reactor used to treat the G-FET. This equipment can discharge both ICP and CCP. The reactor consists of a cylindrical stainless steel chamber. We used Ar as the gas and maintained the pressure at 30 mTorr. A four-turn spiral coil delivered 13.56 MHz radio frequency (rf) power to the Ar gas through the ceramic dielectric at the chamber top, resulting in an ICP discharge. A self-bias negative voltage (V_b) is developed by a 12.50 MHz rf power through the aluminum electrode chuck at the chamber bottom, resulting in a CCP discharge. To cool the G-FET that is exposed to the plasma, cooling water (16 °C) supplied from a chiller was introduced into the cooling line of circular tubing inside the electrode chuck. The G-FET was thermally contacted with the electrode chuck surface by using a thermal paste. A Langmuir probe was introduced into the chamber to estimate the ion density (n_i) and electron temperature (T_e). The distance between the probe and the electrode chuck was fixed at 2.5 cm. Figure 1b shows n_i and T_e for various Ar plasmas. Here, n_i is dramatically decreased to 3.5×10^8 cm^{-3} when the ICP power decreases to 5 W. In general, rf power $\geq$ 100 W is applied to the coil to discharge the ICP in the high plasma density range. In this study, however, we intentionally use 5 W to discharge the ICP in order to run the process at extremely low plasma densities.

Experimental Process. The experimental tools (plasma reactor, semiconductor analyzer, and Raman spectrometer) were located very close to each other, within a distance of ~15 m. Therefore, we managed to perform electrical characterization and Raman analysis within 1 min immediately after plasma treatment. The reason that we have done such controlled and immediate measurements is as follows. It is known that graphene changes to p-type under ambient air from the reaction with oxygen, and electrical properties of graphene after plasma treatment can therefore be affected. However, we tried to minimize the particle-absorbing effect by conducting the electrical measurements immediately after the plasma treatment.

Effect of ICP on Temperature Increase of Graphene. This article deals with the effect of ICP treatment on the temperature of FLG. In the previous report, the surface temperature of Si exposed to ICP (90–245 W) continued to increase with increasing ICP exposure duration without cooling of the substrate electrode.[34,35] However, it is possible to control the saturated temperature as a function of cooling intensity.[43] Therefore, for only 5 W of ICP, the temperature change of any substrate with cooling is very little, and we think that the ICP treatments in this work do not change the material properties of FLG, in contrast to thermal processes such as thermal annealing.

Conflict of Interest: The authors declare no competing financial interest.

Acknowledgment. This research was supported by the Basic Science Research Program through the National Research Foundation of Korea (NRF) funded by the Ministry of Education, Science and Technology (2009-0083540, 2011-0010274).

Supporting Information Available: Figure S1. This material is available free of charge via the Internet at http://pubs.acs.org.

REFERENCES AND NOTES

1. Novoselov, K. S.; Geim, A. K.; Morozov, S. V.; Jiang, D.; Zhang, Y.; Dubonos, S. V.; Grigorieva, I. V.; Firsov, A. A. Electric Field Effect in Atomically Thin Carbon Films. *Science* **2004**, *306*, 666–669.
2. Novoselov, K. S.; Geim, A. K.; Morozov, S. V.; Jiang, D.; Katsnelson, M. I.; Grigorieva, I. V.; Dubonos, S. V.; Firsov, A. A. Two-Dimensional Gas of Massless Dirac Fermions in Graphene. *Nature* **2005**, *438*, 197–200.
3. Zhang, Y. B.; Tan, Y.-W.; Stormer, H. L.; Kim, P. Experimental Observation of the Quantum Hall Effect and Berry's Phase in Graphene. *Nature* **2005**, *438*, 201–204.
4. Schedin, F.; Geim, A. K.; Morozov, S. V.; Hill, E. W.; Blake, P.; Katsnelson, M. I.; Novoselov, K. S. Detection of Individual Gas Molecules Adsorbed on Graphene. *Nat. Mater.* **2007**, *6*, 652–655.
5. Ryu, S.; Liu, L.; Berciaud, S.; Yu, Y. -J.; Liu, H.; Kim, P.; Flynn, G. W.; Brus, L. E. Atmospheric Oxygen Binding and Hole Doping in Deformed Graphene on a SiO_2 Substrate. *Nano Lett.* **2010**, *10*, 4944–4951.
6. Ishigami, M.; Chen, J. H.; Cullen, W. G.; Fuhrer, M. S.; Williams, E. D. Atomic Structure of Graphene on SiO_2. *Nano Lett.* **2007**, *7*, 1643–1648.
7. Dan, Y. P.; Lu, Y.; Kybert, N. J.; Luo, Z. T.; Johnson, A. T. C. Intrinsic Response of Graphene Vapor Sensors. *Nano Lett.* **2009**, *9*, 1472–1475.
8. Cheng, Z. G.; Zhou, Q.; Wang, C.; Li, Q.; Wang, C.; Fang, Y. Toward Intrinsic Graphene Surfaces: A Systematic Study on Thermal Annealing and Wet-Chemical Treatment of SiO_2-Supported Graphene Devices. *Nano Lett.* **2011**, *11*, 767–771.

9. Nourbakhsh, A.; Cantoro, M.; Klekachev, A.; Clemente, F.; Soree, B.; van der Veen, M. H.; Vosch, T.; Stesmans, A.; Sels, B.; Gendt, S. D. Tuning the Fermi Level of SiO_2-Supported Single-Layer Graphene by Thermal Annealing. *J. Phys. Chem. C* **2010**, *114*, 6894–6900.
10. Moser, J.; Barreiro, A.; Bachtold, A. Current-Induced Cleaning of Graphene. *Appl. Phys. Lett.* **2007**, *91*, 163513.
11. Connolly, M. R.; Chiou, K. L.; Smith, C. G.; Anderson, D.; Jones, G. A. C.; Lombardo, A.; Fasoli, A.; Ferrari, A. C. Scanning Gate Microscopy of Current-Annealed Single Layer Graphene. *Appl. Phys. Lett.* **2010**, *96*, 113501.
12. Lin, Y.-C.; Lu, C.-C.; Yeh, C.-H.; Jin, C. H.; Suenaga, K.; Chiu, P.-W. Graphene Annealing: How Clean Can It Be? *Nano Lett.* **2012**, *12*, 414–419.
13. Rider, A. E.; Kumar, S.; Furman, S. A.; Ostrikov, K. Self-Organized Au Nanoarrays on Vertical Graphenes: an Advanced Three-Dimensional Sensing Platform. *Chem. Commun.* **2012**, *48*, 2659–2661.
14. Nandamuri, G.; Roumimov, S.; Solanki, R. Remote Plasma Assisted Growth of Grapheme Films. *Appl. Phys. Lett.* **2010**, *96*, 154101.
15. Seo, D. H.; Kumar, S.; Ostrikov, K. Thinning Vertical Graphenes, Tuning Electrical Response: From Semiconducting to Metallic. *J. Mater. Chem.* **2011**, *21*, 16339.
16. Elias, D. C.; Nair, R. R.; Mohiuddin, T. M. G.; Morozov, S. V.; Blake, P.; Halsall, M. P.; Ferrari, A. C.; Boukhvalov, D. W.; Katsnelson, M. I.; Geim, A. K.; *et al*. Control of Graphene's Properties by Reversible Hydrogenation: Evidence for Graphane. *Science* **2009**, *323*, 610–613.
17. Hopkins, P. E.; Baraket, M.; Barnat, E. V.; Beechem, T. E.; Kearney, S. P.; Duda, J. C.; Robinson, J. T.; Walton, S. G. Manipulating Thermal Conductance at Metal−Graphene Contacts via Chemical Functionalization. *Nano Lett.* **2012**, *12*, 590–595.
18. Bai, J.; Duan., X.; Huang, Y. Rational Fabrication of Graphene Nanoribbons Using a Nanowire Etch Mask. *Nano Lett.* **2009**, *9*, 2083–2087.
19. Xie, L.; Jiao, L.; Dai, H. Selective Etching of Graphene Edges by Hydrogen Plasma. *J. Am. Chem. Soc.* **2010**, *132*, 14751–14753.
20. Lin, Y.-C.; Lin, C.-Y.; Chiu, P.-W. Controllable Graphene N-Doping with Ammonia Plasma. *Appl. Phys. Lett.* **2010**, *96*, 133110.
21. Wu, J.; Xie, L.; Li, Y.; Wang, H.; Ouyang, Y.; Guo, J.; Dai, H. Controlled Chlorine Plasma Reaction for Noninvasive Graphene Doping. *J. Am. Chem. Soc.* **2011**, *133*, 19668–19671.
22. Nourbakhsh, A.; Cantoro, M.; Vosch, T.; Pourtois, G.; Clemente, F.; van der Veen, M. H.; Hofkens, J.; Heyns, M. M.; Gendt, S. D.; Sels, B. F. Bandgap Opening in Oxygen Plasma-Treated Graphene. *Nanotechnology* **2010**, *21*, 435203.
23. Shin, Y. J.; Wang, Y.; Huang, H.; Kalon, G.; Wee, A. T. S.; Shen, Z.; Bhatia, C. S.; Yang, H. Surface-Energy Engineering of Graphene. *Langmuir* **2010**, *26*, 3798–3802.
24. Choi, M. S.; Lee, S. H.; Yoo, W. J. Plasma Treatments to Improve Metal Contacts in Graphene Field Effect Transistor. *J. Appl. Phys.* **2011**, *110*, 073305.
25. Gokus, T.; Nair, R. R.; Bonetti, A.; Bohmler, M.; Lombardo, A.; Novoselov, K. S.; Geim, A. K.; Ferrari, A. C.; Hartschuh, A. Making Graphene Luminescent by Oxygen Plasma Treatment. *ACS Nano* **2009**, *3*, 3963–3968.
26. Xiao, N.; Dong, X.; Song, L.; Liu, D.; Tay, Y. Y.; Wu, S.; Li, L.-J.; Zhao, Y.; Yu, T.; Zhang, H.; *et al*. Enhanced Thermopower of Graphene Films with Oxygen Plasma Treatment. *ACS Nano* **2011**, *5*, 2749–2755.
27. Xu, S.; Ostrikov, K. N.; Li, Y.; Tsakadze, E. L.; Jones, I. R. Low-Frequency, High-Density, Inductively Coupled Plasma Sources: Operation and Applications. *Phys. Plasmas* **2001**, *8*, 2549–2557.
28. Kim, K.; Choi, J.-Y.; Kim, T.; Cho, S.-H.; Chung, H.-J. A Role for Graphene in Silicon-Based Semiconductor Devices. *Nature* **2011**, *479*, 338–344.
29. Lieberman, M. A.; Lichtenberg, A. J. *Principles of Plasma Discharges and Materials Processing*; Wiley Interscience: New York, 1994; p 165.
30. Denpoh, K.; Ventzek, P. L. G. Test Particle Simulation of the Role of Ballistic Electrons in Hybrid dc/rf Capacitively Coupled Plasmas in Argon. *J. Vac. Sci. Technol. A* **2008**, *26*, 1415–1424.
31. Lehtinen, O.; Kotakoski, J.; Krasheninnikov, A. V.; Tolvanen, A.; Nordlund, K.; Keinonen, J. Effects of Ion Bombardment on a Two-Dimensional Target: Atomistic Simulations of Graphene Irradiation. *Phys. Rev. B* **2010**, *81*, 153401.
32. Davis, W. D.; Vanderslice, T. A. Ion Energies at the Cathode of a Glow Discharge. *Phys. Rev.* **1963**, *131*, 219–228.
33. Gao, F.; Zhao, S.-X.; Li, X.-S.; Wang, Y.-N. Comparison Between Experiment and Simulation for Argon Inductively Coupled Plasma. *Phys. Plasmas* **2009**, *16*, 113502.
34. Hsu, C. C.; Titus, M. J.; Graves, D. B. Measurement and Modeling of Time- and Spatial-Resolved Wafer Surface Temperature in Inductively Coupled Plasmas. *J. Vac. Sci. Technol. A* **2007**, *25*, 607–614.
35. Titus, M. J.; Graves, D. B. Wafer Heating Mechanisms in a Molecular Gas, Inductively Coupled Plasma: *in situ*, Real Time Wafer Surface Measurements and Three-Dimensional Thermal Modeling. *J. Vac. Sci. Technol. A* **2008**, *26*, 1154–1160.
36. Wolf, S.; Tauber, R. N. *Silicon Processing for the VLSI Era*; Lattice Press: CA, 1986.
37. Li, X.; Cai, W.; An, J.; Kim, S.; Nah, J.; Yang, D.; Piner, R.; Velamakanni, A.; Jung, I.; Tutuc, E.; *et al*. Large-Area Synthesis of High-Quality and Uniform Graphene Films on Copper Foils. *Science* **2009**, *324*, 1312–1314.
38. Pirkle, A.; Chan, J.; Venugopal, A.; Hinojos, D.; Magnuson, C. W.; McDonnell, S.; Colombo, L.; Vogel, E. M.; Ruoff, R. S.; Wallace, R. M. The Effect of Chemical Residues on the Physical and Electrical Properties of Chemical Vapor Deposited Graphene Transferred to SiO_2. *Appl. Phys. Lett.* **2011**, *99*, 122108.
39. Mohiuddin, T. M. G.; Lombardo, A.; Nair, R. R.; Bonetti, A.; Savini, G.; Jalil, R.; Bonini, N.; Basko, D. M.; Galiotis, C.; Marzari, N.; *et al*. Uniaxial Strain in Graphene by Raman Spectroscopy: *G* peak Splitting, Grüneisen Parameters, and Sample Orientation. *Phys. Rev. B* **2009**, *79*, 205433.
40. Calizo, I.; Balandin, A. A.; Bao, W.; Miao, F.; Lau, C. N. Temperature Dependence of the Raman Spectra of Graphene and Graphene Multilayers. *Nano Lett.* **2007**, *7*, 2645–2649.
41. Giovannetti, G.; Khomyakov, P. A.; Brocks, G.; Karpan, V. M.; van den Brink, J.; Kelly, P. J. Doping Graphene with Metal Contacts. *Phys. Rev. Lett.* **2008**, *101*, 026803.
42. Tapaszto, L.; Dobrik, G.; Nemes-Incze, P.; Vertesy, G.; Lambin, Ph.; Biro, L. P. Tuning the Electronic Structure of Graphene by Ion Irradiation. *Phys. Rev. B* **2008**, *78*, 233407.
43. Gabriel, C. T. Wafer Temperature Measurements During Dielectric Etching in a MERIE Etcher. *J. Vac. Sci. Technol. B* **2002**, *20*, 1542–1547.